Taylor & Francis
Taylor & Francis Group

# Ultimate strength models for spherical shells under external pressure: a comparative study

## Liang Zhao & Yong Bai

Taylor & Francis
Taylor & Francis Group

Check for updates

# Ultimate strength models for spherical shells under external pressure: a comparative study

Liang Zhao ⬥ and Yong Bai

College of Civil Engineering and Architecture, Zhejiang University, Hangzhou, People's Republic of China

**ABSTRACT**

The ultimate strength of spherical shells under external pressure has been an attractive topic in the field of marine structures. However, recent studies have revealed that the current theoretical approaches are hardly compatible with the actual hulls, which indicates that the ultimate strength models still need to be reevaluated and unified. To address this challenge, a comparative study has been conducted in this paper. Various analytical approaches and codified rules are compared through screened experiment data that have realistic imperfections and different shape parameters in the range generally applied for marine structures. The model evaluation criteria have been established by implementing statistical model uncertainty factors in terms of bias and coefficient of variation. A comparison of the results has been made from three different aspects including shell shape, $R/t$ and geometrical parameters to evaluate their performance. Based on the calculation outcome, analysis has been made to study the theory behind those models and determine their limitations and recommended application range.

## Nomenclature

| | |
|---|---|
| $R$ | middle mean radius of the spherical shell |
| $t$ | wall thickness |
| $\nu$ | Poisson's ratio |
| $P_{cr}$ | buckling pressure of the spherical shell |
| $P_e$ | elastic buckling pressure of the spherical shell |
| $P_y$ | yield pressure of the spherical shell, $P_y = 2(t/R)\,\sigma_y$ |
| $P_{exp}$ | experimental collapse pressure |
| $E$ | modulus of elasticity |
| $\sigma_y$ | yield point of the material |
| $\phi$ | semi-vertex angle |
| $\lambda$ | geometrical parameter |
| $\delta_0$ | local radial imperfection |
| $\overline{\lambda_s}$ | slenderness parameter, $\overline{\lambda_s} = 1.258\sqrt{(R/t)(\sigma_y/E)}$ |

## 1. Introduction

The ultimate strength of spherical shells and spherical caps under external pressure has been an intriguing subject for a long history. Spherical shells (see Figure 1) are common structural components for various types of marine structures including deep manned submersibles, tanks and domed closures. They find extensive applications from deep-sea exploration to liquid gas transportation (Zhao, Wang, et al. 2022; Zhao, Bai, et al. 2022). To achieve the reliable design of marine structures, it is crucial to establish a good ultimate strength model for spherical shells (Zhang et al. 2021; Zhu et al. 2021; Bagheri et al. 2022; Zhang et al. 2022).

The ultimate strength models of spherical shells have been widely studied through either one of the analytical, numerical and experimental approaches or their combinations (Zhang et al. 2019). Evkin et al. (2017), Evkin (2019), and Evkin and Lykhachova 2019) extended their early research on cylindrical shells (Evkin et al. 1978) and proposed a stability estimation formula for spherical shells based on the energy barrier criterion (EBC). Experiment and numerical results have supported the estimation and it is suggested for buckling design (Evkin 2019). Another attempt is based on a robust knockdown factor which is developed for a reliable design for various thin-wall shells (Wagner et al. 2017,

2018a, 2018b). Validation results have shown that it presents much more aggressive predictions when $\lambda < 10$ compared to Evkin and Lykhachova (2019). Numerical model and experimental investigations on spherical caps were conducted by Wang, Tang, et al. (2019) and Wang et al. (2020). Their proposed nonlinear risk algorithm is in good agreement with experimental results; however, this method is limited in predicting caps made from stainless steel. Moreover, Zhu et al. (2020) proposed a formula to predict the local buckling of corroded spherical shells by considering the wall thickness reduction due to the local corrosion. Similar work was presented by Zhao, Zhang, et al. (2022), both numerical and analytical approaches are proposed to predict the reduction factor of collapse pressure for the local corroded shells.

However, comparative studies have been carried out between current strength models or design rules (Pan and Cui 2011; Wagner et al. 2018b; Zhang et al. 2019; Evkin 2019). According to their calculation, the results given by the theoretical approaches are hardly compatible with the actual hulls, which indicates that the ultimate strength models for spherical shells still need to be reevaluated and unified. Moreover, the basic consideration of establishing the strength models for shell structures is quite complicated primarily due to the greater stockiness in configuration (Das et al. 2003). In general, the model must take the yield (collapse) mode and the buckling mode into consideration. Also, the effects of imperfection, which is common for all shell structures and residual stresses, particularly pronounced in fabricated metal structures, should be considered. The numerical approaches can cater to most of these considerations but they are time–cost and need to be evaluated before real application, which makes it not feasible for the initial design. Therefore, analytical approaches are often preferable for establishing strength models.

In this paper, a comparative study has been conducted to evaluate the current strength models for spherical shells with screened experiment data. In Section 2, the model evaluation criteria are established by implementing statistical model uncertainty factors in terms of bias and COV. Section 3 presents the basics of ultimate
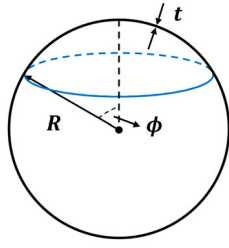
**Figure 1.** The geometry of a spherical shell. (This figure is available in colour online.)

strength for spherical shells. The strength models are listed in Section 4. In Section 5, comparisons and analyses are conducted from different aspects to evaluate the formulations. Finally, Section 6 contains the conclusion of the research.

## 2. Model evaluation criteria

One of the most convenient ways to evaluate the model uncertainty is to compare the experimental results with theoretical predictions. We choose the statistical mean bias $X_m$ and coefficient of variance COV to evaluate the general performance of a certain model, see Equations (1) and (2):

$$X_m = \frac{\text{experiment value}}{\text{predicted value}} \quad (1)$$

$$COV = \sqrt{\frac{\sum_{i=1}^{n}(X_i - X_m)}{n}} / X_m \quad (2)$$

where $n$ is the number of testing samples. $X_m$ reflects the average performance of the model, while COV shows the departure degree of the dataset from the average. It is worth mentioning that for a good strength model, the mean bias should tend to unity, while the COV should be as small as possible.

## 3. Buckling of spherical shells

There are two possible failure modes for an ideal spherical shell: the plastic collapse and elastic (or elastic-plastic) buckling. The former occurs when the maximum stress in the shell reaches the material yield point which results in a plastic collapse $P_y$, while the latter one occurs when the stress reaches the critical buckling pressure $P_e$, which is given by Zoelly (1915), see Equation (3). The minimum pressure of these two failure modes is defined as the ultimate strength of the spherical shell. Comparing these two buckling modes, one can see that the ultimate strength mainly depends on the material property and the ratio $t/R$. Pan and Cui (2010) gave a calculation example of a titanium shell, when $t/R$ is less than 0.013 the ultimate strength falls into an elastic mode, while $t/R$ is larger than 0.013 and falls into another mode. It is calculated under some ideal assumptions but it still indicates the ultimate

**Table 1.** Comparison between experimental results and theoretical prediction.

| Model | Experimental Collapse Pressure $P_{exp}$ (Mpa) | Predicted by (3) (Mpa) |
|---|---|---|
| SS-1 | 97.733 | 798.741 |
| SS-2 | 98.250 | 792.788 |
| SS-3 | 58.605 | 330.441 |
| SS-4 | 56.365 | 315.435 |
| SS-5 | 19.995 | 53.887 |
| SS-6 | 20.340 | 52.833 |
| SS-7 | 7.584 | 14.046 |
| SS-8 | 7.575 | 13.733 |

strength model should account for two buckling modes to predict a shell failure with arbitrary $t/R$ and material.

$$P_e = \frac{2E}{\sqrt{3(1-v^2)}}\left(\frac{t}{R}\right)^2 \quad (3)$$

However, the ideal spherical shells do not exist in reality. Many experimental studies have revealed that the actual buckling pressure is always less than the value given by Equation (3). The buckling experiment carried out by Krenzke and Kiernan (1963) has shown how the experiment data differed from the theoretical prediction, see Table 1. One reason is that Equation (3) only considers the buckling that happens in the elastic phase of the material, while the impact of nonlinear behaviour is ignored. The calculation presented by Zhang et al. (2015) revealed that the error of Equation (3) will get larger as the thickness-to-radius ratio increases, and it is because the buckling of thick shells is significantly influenced by the yield strength.

Another reason is the buckling pressure of spherical shells is highly imperfection-sensitive (Thompson and Sieber 2016). Geometrical imperfections are defined as shape deviations from the ideal structure and have been identified as one of the main causes of low buckling loads of shells. The shapes of the imperfections are usually defined based on measured geometric imperfection (Wagner et al. 2018b), which are theoretically to be predicted as dimple-like imperfections, linear buckling mode-shape imperfections (eigenmode imperfections), Legendre polynomials and increased radius. Galletly and Blachut (1991) and Galletly et al. (1987) revealed that the Legendre polynomial causes a greater reduction than the increased radius. Błachut (2015) compared these four types of imperfections and found that force-induced dimple is the 'worst' imperfection among them, which is agreed by the results from Arbelo et al. (2014). Nevertheless, a comparative study made by Wang, Tang, et al. (2019) shown eigenmode imperfection (see Figure 2) is the most conservative one, which contradicts the previous findings. The attempt to search for the worst-case scenario imperfection has not yet reached a general status and agreement.

## 4. Strength models for spherical shells

### 4.1. Formulae presented by Russian maritime register of shipping (RS)

The equation given by the Russian Maritime Register of Shipping (2018) is mainly based on the theory of Paliy (1991), see Equation (4).

$$P_{cr} = \eta_s P_e \quad (4)$$

In Equation (4) $\eta_s$ is the coefficient that represents the nonlinear behaviour of the material and geometrical imperfections. It can be calculated according to the following equation:

$$\eta_s = \frac{\eta_{1s}}{\sqrt{1 + \eta_{1s}\delta^2[af_s + \eta_{1s}(1+f_s)^2]}} \quad (5)$$

$$\delta = \frac{P_e}{P_y} \quad (6)$$

$$\eta_{1s} = \frac{1}{1 + (2.8 + f_s)f_s^{2/3}} \quad (7)$$

$$f_s = \frac{f}{t} \quad (8)$$

$$a = \begin{cases} 0 & , \ f_s \leq 0.1 \\ 2\sqrt{f_s - 0.1} & , \ f_s > 0.1 \end{cases} \quad (9)$$
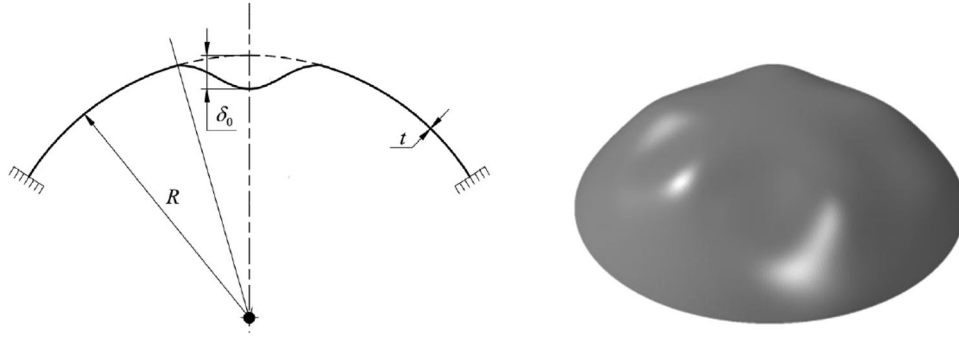
**Figure 2.** Dimple-like imperfection (left) and eigenmode imperfection (right).

In Equations (5)–(8), $\eta_{1s}$, $\delta$ and $f_s$ are coefficients that can be calculated separately. $f$ denotes the local maximum deviation of the spherical shell. The coefficient $a$ is determined in Equation (9).

### 4.2. Formula presented by American Bureau of Shipping (ABS)

The formulations presented by the American Bureau of Shipping (2021) mainly depend on the ratio of elastic buckling pressure $P_e$ to yield load $P_y$. When $P_e/P_y > 1$, the spherical shell will collapse due to the stress in the shell reaching the yield point, which usually happens in shells with large thicknesses. When $P_e/P_y \leq 1$, the buckling pressure is controlled by the elastic buckling, as shown in the following equation:

$$P_{cr} = P_{cs} sf \qquad (10)$$

$$\frac{P_{cs}}{P_y} = \begin{cases} 0.7391\{1 + [P_y/(0.3P_e)]^2\}^{-1/2}, & P_e/P_y > 1 \\ \dfrac{0.2124P_e}{P_y}, & P_e/P_y \leq 1 \end{cases} \qquad (11)$$

In Equation (10), $sf$ denotes the safety factor, which is 0.67.

### 4.3. Formula presented by Det Norske Veritas (DNV)

Similar to the ABS code, the formulations given by DNV (2021) also depend on the ratio of $P_e/P_y$. The primary calculation equations of DNV are Equations (12) to (14)

$$P_{cr} = P_e \quad \text{if } P_e/P_y \leq 0.47 \qquad (12)$$

$$P_{cr} = P_y \left( 0.38 + 0.195 \frac{P_e}{P_y} \right) \quad \text{if } 0.47 < P_e/P_y \leq 3.18 \qquad (13)$$

$$P_{cr} = P_y \quad \text{if } P_e/P_y > 3.18 \qquad (14)$$

### 4.4. Formula presented by NASA

The formulation is, as follows, as proposed by NASA (1969), which is based on the lower bound for a large amount of experiment data. The experimental buckling pressure values are represented by means of a knockdown factor (KDF) which is defined as the ratio of the buckling pressure $P_{exp}$ of a real experiment test shell to the theoretical buckling pressure $P_e$, see Equation (15).

$$\rho = \frac{P_{exp}}{P_e} \qquad (15)$$

These KDFs are plotted against the shell shape parameter $\lambda$ which is defined according to Equation (16).

$$\lambda = [12(1 - v^2)]^{1/4}(R/t)^{1/2}2\sin(\frac{\phi}{2}) \qquad (16)$$

The KDF given by NASA SP-8032 which represents a statistically lower bound of different empirical data is defined as Equation (17).

$$\rho = 0.14 + \frac{3.2}{\lambda^2} \qquad (17)$$

Then the ultimate strength can be calculated by the following equation:

$$P_{cr} = P_e \cdot \rho \qquad (18)$$

Evkin and Lykhachova (2017) and Wagner et al. (2018b) have shown that the NASA SP-8032 recommendation is a very conservative estimation of the buckling pressure of spherical shells.

### 4.5. Formula presented by Wagner

Wagner et al. (2018b) proposed a new type of imperfection known as perturbation cutouts to replace the traditional measure-based imperfections. Implementing the equivalent geometric imperfections and plastic nonlinear analysis, a lower bound buckling pressure curve is obtained as follows:

$$\rho = 5.172\lambda^{-1.464} + 0.1296 \qquad (19)$$

Therefore, the buckling pressure of spherical shells under external pressure can be approximated by Equation (18). However, the equation is mostly valid under some conditions:

- $\lambda > 5.5$
- Linear elastic and isotropic material behaviour
- Clamped boundary conditions

The new knockdown factors are validated with a large collection of different test data and the results show that the experimental knockdown factors of nearly all shells can be predicted very well with the new design procedure (Wagner et al. 2018b).

### 4.6. Formula presented by Evkin

Evkin (2019) extended the Energy Barrier Criteria (Evkin and Lykhachova 2017) to the case of spherical shells. It is developed for shells with geometrical imperfections for the design buckling load of spherical structures. They suggested the following

**Table 2.** The test data excluded from the model.

| Models | Recommended range reported in the literature | Our range | The number of results should be excluded |
|---|---|---|---|
| Wagner et al. (2018b) | $\lambda > 5.5$ | 2.3-81.7 | 10 |
| Evkin (2019) | $\lambda \geq 5$ | 2.3-81.7 | 10 |
| Galletly and Blachut (1991) | Steel and aluminium | Maraging steel; Titanium alloy | 6 |
| DNV (2021) | Ferritic steel or similar | Maraging steel; Titanium alloy | 6 |

estimation:

$$\rho = \frac{0.693}{(1-\nu)^{0.2}\lambda^{0.4}} \left( 1 - 0.2(\lambda - 3.5)e^{-\frac{\lambda - 3.5}{3.95}} \right) \quad (20)$$

Similar to the previous equation, the ultimate strength can be calculated according to Equation (18). The formulation given by Evkin extended the application range compared to Equation (19). The situation when $\lambda < 5.5$ is considered in the model. The advantage of this approach is considering not only geometrical imperfections but also external perturbations including boundary moments.

### 4.7. Formula presented by Galltely

Another equation given by Galletly and Blachut (1991) is derived numerically from collapse pressures predicted by the computer program BOSOR 5. It considers both the increased radius and the Legendre polynomial imperfections. The equations may seem old and complicated but it actually reaches relatively good calculation results. The formulations are presented as follows:

$$\frac{P_{cr}}{P_y} = \frac{1 + 0.084e^{[-20(\bar{\lambda}-1.07)^2]}}{\sqrt{1 + \bar{\lambda}^{4.3}}} K(\bar{\lambda}, \ \delta_0/t) \quad (21)$$

where

$$\frac{1}{K(\bar{\lambda}, \ \delta_0/t)} = \sqrt{1 + [12.9 + 3.275 sinh^{-1}15(\bar{\lambda} - 0.75)](\delta_0/t)^{1.51}} \quad (22)$$

The comparison between the test results and the formula shows that it could be given for the lower bound curve in terms of $\bar{\lambda}$.

## 5. Test results and comparison

### 5.1. Description of experiment data

To evaluate the current strength models, it is first necessary to substantiate the relevant experimental tests. For the comparative study, one of the most convenient ways to deal with model uncertainty is to compare experimental results with the model prediction. The tested data considered in this study are taken from various existing test data references. However, before validating any theoretical formulation, we found some of the data are not compatible with our

methods. First, some of these models are obtained with a specific interpolating range. Thus, the experiment results that are not in the recommended range reported by the literature should be excluded. Table 2 presents the data excluded for each model. Second, some of the specimen results showed a very large knock-down factor and we decide to exclude them. These test results are useless because the shells with high buckling pressure indicate no geometrical imperfections which are essential for our study. Besides, it is worth mentioning that some of the experiment does not report the geometrical imperfections; therefore, we fill them with the maximum imperfection tolerances permitted by DNV (2021).

Table 3 shows the basic information of the experiment data we gleaned. Also, more detailed experimental results are presented in Appendix. Most shells are in the range of $\lambda > 5.5$ which was first determined by Huang (1964). In this region, the unsymmetrical buckling starts to appear and it is usually with a relatively higher R/t ratio. However, some of the experiment data fall into the second region when $\lambda < 5.5$. In this range, the specimens are usually thick-wall shells and their buckling behaviour is significantly influenced by material plasticity. The region $\lambda < 5.5$ is defined as 'Budiansky-range' and the region for $\lambda > 5.5$ is defined as 'Huang-range' for the following discussion. It is worth mentioning that these specimens are made of different materials from high-strength metal (Titanium, Maraging steel) to relatively low-strength material (Aluminium, stainless steel). Also, since the manufacturing technology will greatly influence the quality of the specimens, we have chosen the experiment data from the literature after 1950. In the next section, a comparative study will be conducted to evaluate the models with these experimental results.

### 5.2. Test results

The calculation results of the experimental data are shown in Table 4. It is worth mentioning that the results given by Kołodziej and Marcinowski (2018) show a significantly large deviation from the experiment data (some of the bias even larger than 4). The reason for this is mainly because the specimens in the literature have a relatively high radius-to-thickness ratio (5–12 times the average R/t), which will cause a significant reduction in the buckling pressure. Moreover, this level of R/t is dominated by the elastic buckling mode, while the current models consider the influence of plastic buckling; therefore, the prediction value is much higher than the

**Table 3.** Properties of experimental data.

| Reference | Qty | Material | Shape | R/t | lambda |
|---|---|---|---|---|---|
| Krenzke and Kiernan (1963) | 30 | Aluminium | Caps/Spheres | 10.4-166.7 | 2.3-31.9 |
| Pan et al. (2012) | 4 | Titanium | Spheres | 25.9-29.7 | 18.5-19.8 |
| Zhang et al. (2017) | 9 | 304 Stainless Steel | Spheres | 103.4-185.9 | 37.2-49.8 |
| Zhang et al. (2018a) | 4 | 304 Stainless Steel | Spheres | 138.9-151.5 | 42.8-44.6 |
| Wang, Zhang, et al. (2019) | 1 | Maraging Steel | Spheres | 28.9 | 19.5 |
| Zhu et al. (2019) | 5 | 304 Stainless Steel | Caps | 136.2-144.7 | 30.1-31.0 |
| Zhang et al. (2018b) | 6 | 304 Stainless Steel | Caps | 86.5-88.0 | 15.3-15.4 |
| Zhang et al. (2019) | 1 | Maraging Steel | Caps | 26.3 | 13.3 |
| Kolodziej and Marcinowski (2018) | 20 | DC04 Steel | Caps | 324.8-1010.6 | 46.3-81.7 |
| Total | 80 | / | / | 10.4-1010.6 | 2.3-81.7 |

**Table 4.** Calculation results.

| Method | Mean | COV |
|---|---|---|
| RS | 1.29 | 0.32 |
| ABS | 1.14 | 0.30 |
| DNV | 0.99 | 0.19 |
| NASA | 1.64 | 0.37 |
| Wagner | 1.27 | 0.31 |
| Evkin | 1.40 | 0.34 |
| Gattely | 1.29 | 0.30 |

experiment due to the plasticity. Also, these specimens are rarely adopted by the marine structure design, so we have eliminated the results to achieve a more reasonable calculation.

The comparison between the experiment and theoretical results was statistically modelled by the mean value of bias and coefficient of variance. Under the model evaluation criteria established in Section 2, the model given by DNV provides a more accurate prediction by the mean and COV, which are 0.99 and 0.19, respectively. The other results show that models from RS, ABS, NASA, Wagner, Evkin and Galletly are less accurate with the mean values of 1.29, 1.14, 1.64, 1.27, 1.40 and 1.29 and the COV values are 0.32, 0.30, 0.37, 0.31, 0.34 and 0.30, respectively. In general, there is plenty of room to improve the models as mentioned above due to the non-unity for bias and large uncertainty in the evaluation.

For a closer look at the models, the results for each formula are compared in the box–whisker plot, see Figure 3. It's clear to see that the ABS code, DNV code and formulae given by Galletly presented a relatively better distribution with less abnormal data. Nevertheless, the models given by RS, NASA, Wagner and Evkin have shown bad performance with many abnormal results (some of the biases are even less than 0.1, while some surpass 4). And a more interesting thing is that these outliers are basically from the same source, which indicates that there may exist some similarities shared by these formulations. The principles behind this phenomenon will be discussed in the later section.
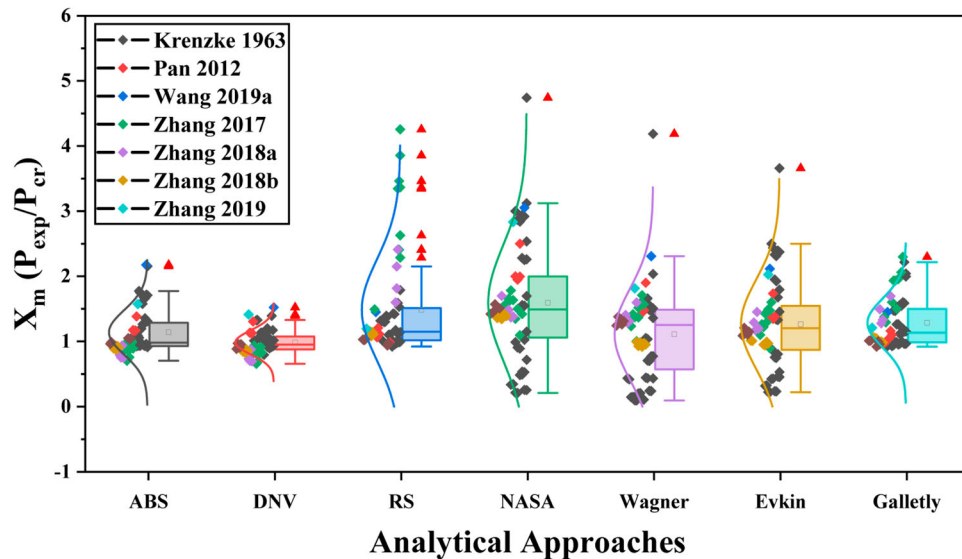


**Figure 3.** Box-whisker plot of the results. (This figure is available in colour online.)
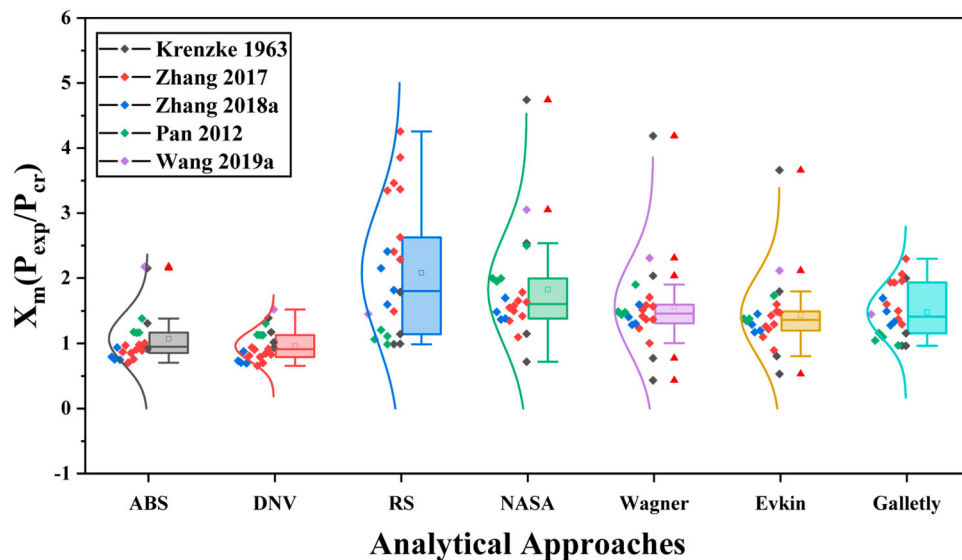


**Figure 4.** Box-whisker plot for results of complete spherical shells. (This figure is available in colour online.)
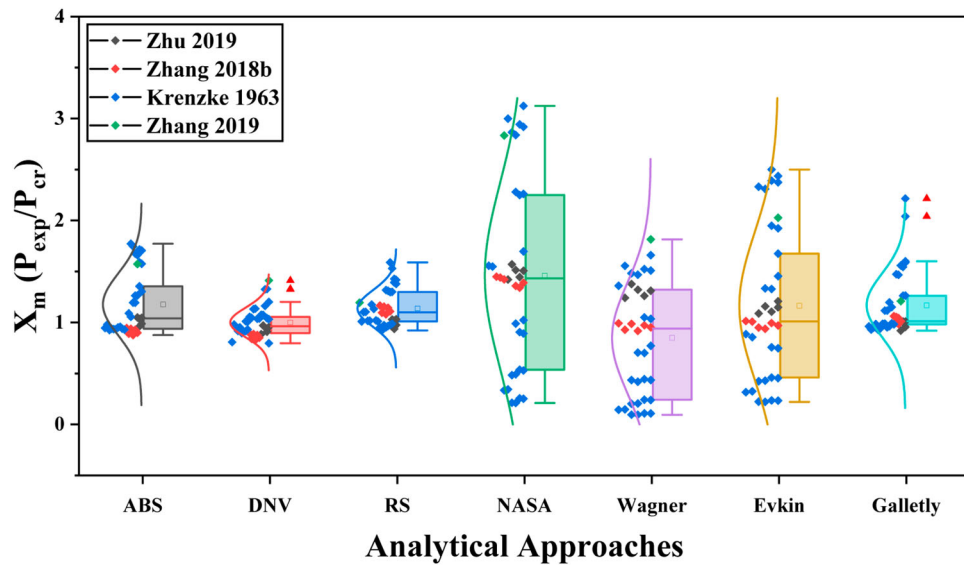
**Figure 5.** Box-whisker plot for results of spherical caps. (This figure is available in colour online.)



(a)

(b)

**Figure 6.** Strength analysis of formula given by the ABS code (left *R/t*; right *λ*). (This figure is available in colour online.)



(a)

(b)

**Figure 7.** Strength analysis of formula given by the DNV code (left *R/t*; right *λ*). (This figure is available in colour online.)

**Figure 8.** Strength analysis of formula given by the RS code (a) by *R/t*; (b) by λ. (This figure is available in colour online.)



**Figure 9.** Strength analysis of formula given by Galletly (left *R/t*; right λ). (This figure is available in colour online.)
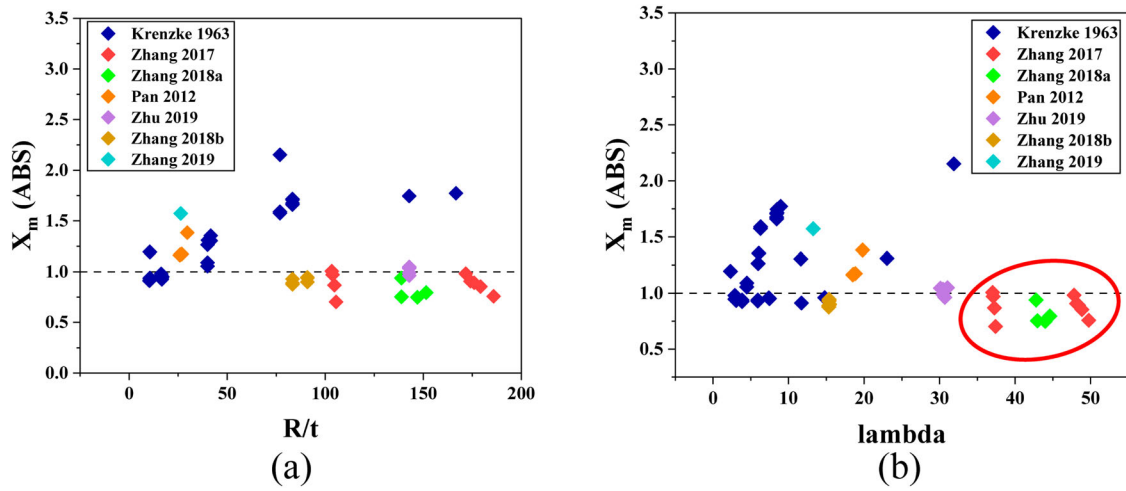


**Figure 10.** Strength analysis of formula given by NASA (left *R/t*; right λ). (This figure is available in colour online.)
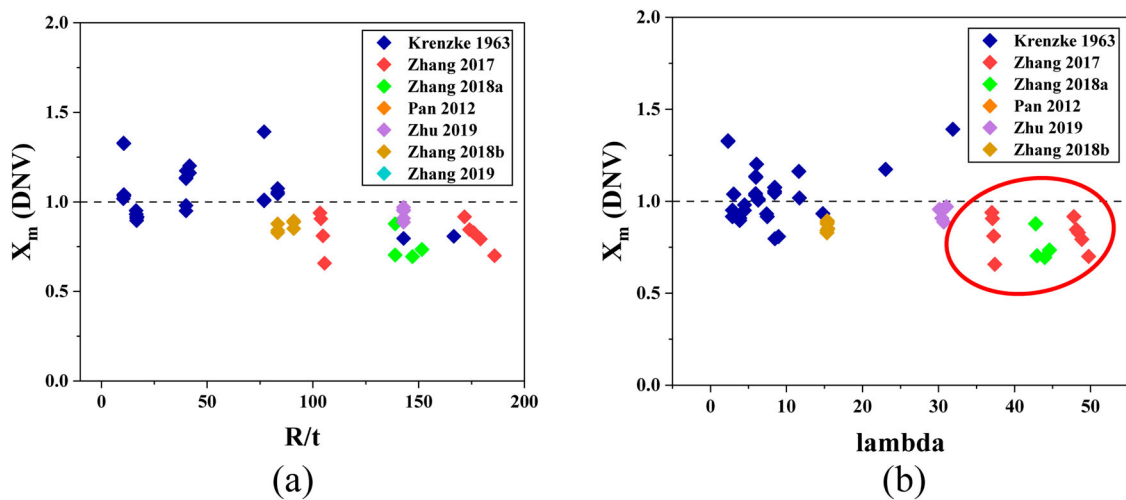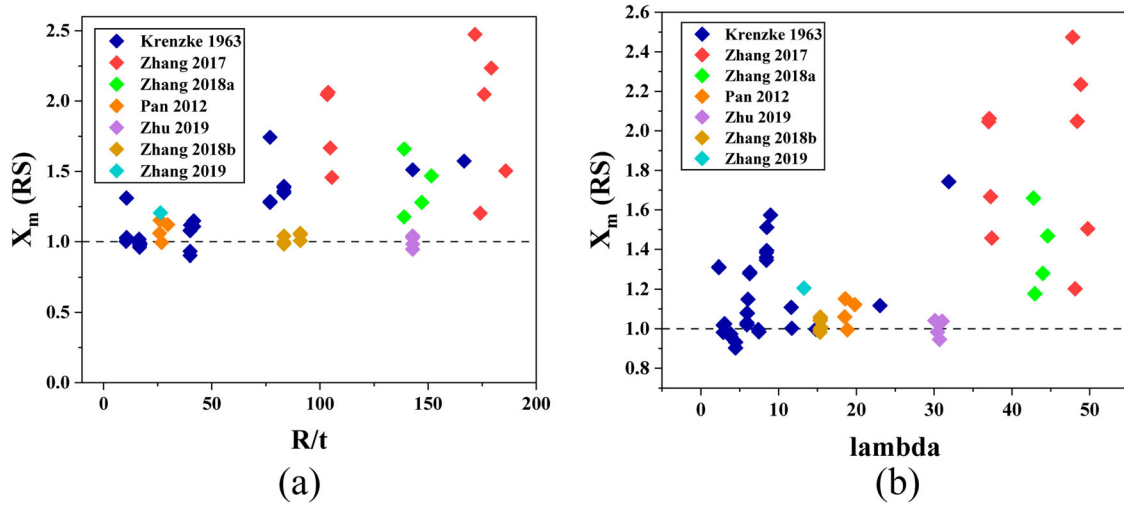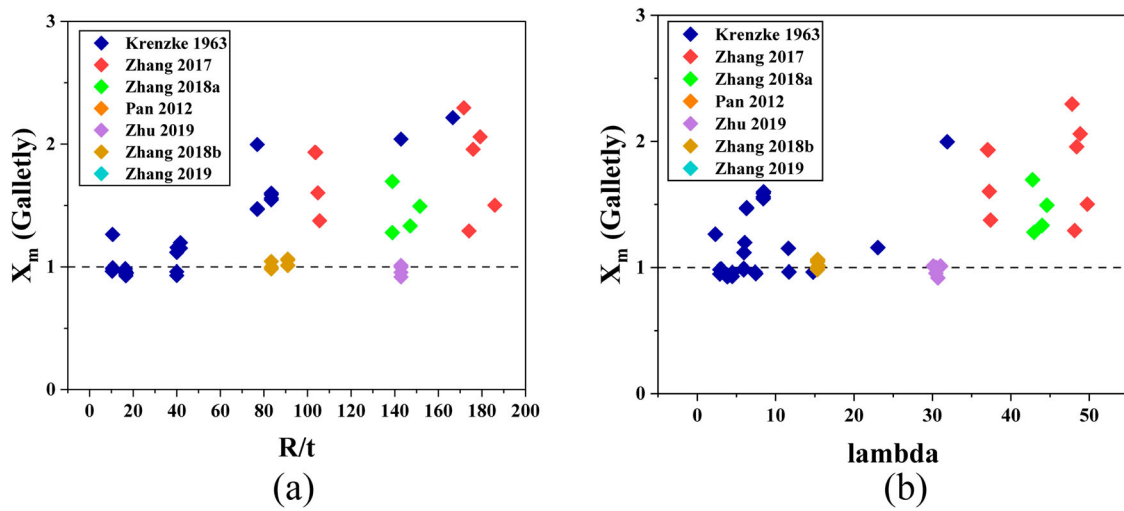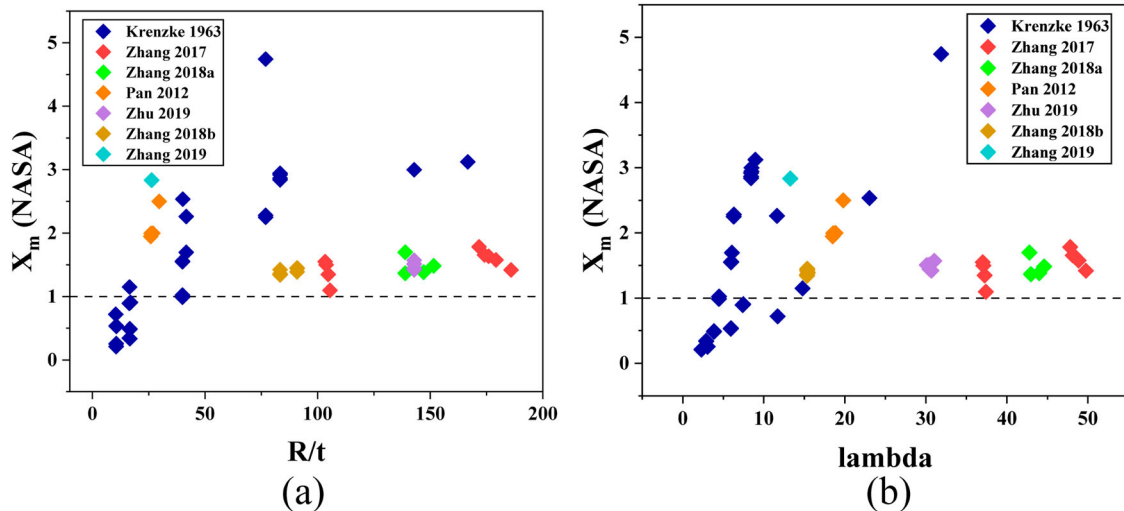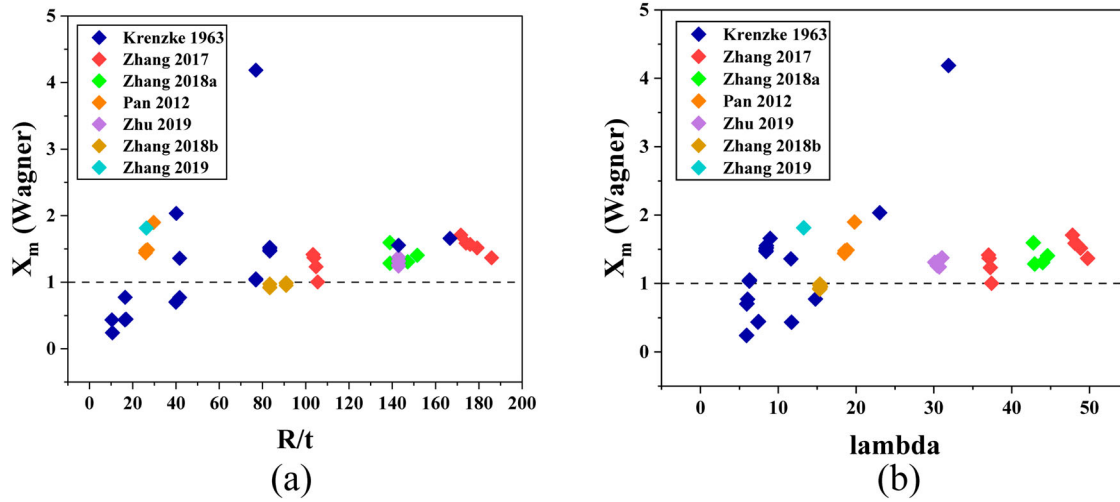
**Figure 11.** Strength analysis of formula given by Wagner (left *R/t*; right λ). (This figure is available in colour online.)

### 5.3. Comparison and analysis

The buckling behaviour does not work the same between complete spheres and spherical caps, which indicates that experiment results would vary even if the specimens share the same parameters and material properties. According to Evkin and Lykhachova. (2017), the buckling pressure for spherical caps would reduce by 20% in the design process compared to complete spherical shells. Therefore, the depth of the shell (dome height) is a crucial factor for ultimate strength prediction. However, most of the formulations we presented above do not mention the effects of dome height, which indicates that they would show different performances predicting the ultimate strength of spheres and caps.

Figures 4 and 5 show the box–whisker plot for the results of complete spherical shells and spherical caps. The graph shows that formulas given by NASA, Wagner and Evkin have shown significantly better performance in spheres than caps. The reasons for the poor results of caps are, the boundary condition of the caps does not perfectly fit the assumptions made by these formulas. These models require the boundary condition must be clamped (for Wagner and NASA) and clamped or hinged (for Evkin); otherwise, the geometric nonlinear would affect the accuracy. The shape

parameters of some specimens are in the Budiansky range, which explains the lower points drawn under these models in Figure 5. Since these assumptions are not satisfied, the drawbacks of the three models in the prediction of spherical caps are revealed. RS code, however, presents an opposite outcome which shows poor performance in predicting spheres. There are two explanations. First, the RS code does not consider the effect of dome height which leads to an over-conservative prediction for complete spherical shells. Another explanation is for the higher results plotted in Figure 5, which come from Zhang et al. (2017). They have relatively larger local imperfections according to the literature. Therefore, the coefficients that represent the imperfection such as $f_s$ in Equation (7) and $a$ in Equation (9) cause a great reduction in $\eta_s$, which explains the large deviation of these data.

The radius to thickness ratio $R/t$ and shape parameter $\lambda$ represents the geometric property of shells. They are deeply connected to the buckling pressure of spherical shells. Comparing the results according to these two parameters could present a comprehensive view of the model performance.

As shown in Figures 6 and 7, the results given by the ABS code and DNV code show a fairly good distribution. First, they obtained
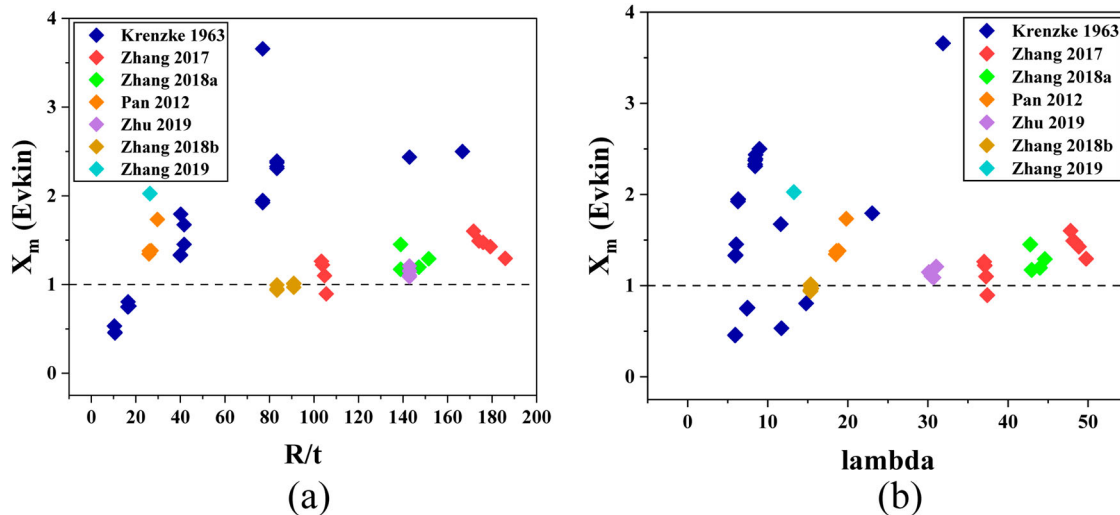


**Figure 12.** Strength analysis of formula given by Evkin (left *R/t*; right λ). (This figure is available in colour online.)

**Table 5.** Conclusion of the comparative study.

| Models | Features and recommended application range |
| --- | --- |
| ABS (2021 ); DNV (2021) | Relatively good approximation with the experiments; |
| | Imperfection value shouldn't exceed the tolerance as an a priori condition; |
| | ABS is better with complete shells than spherical caps while DNV is good with both |
| RS (2018); Galletly and Blachut (1991) | They are both highly imperfection-sensitive models; |
| | The specimen with low manufacture quality is not recommended using these models |
| | RS is much better with spherical caps than complete shells, while Galletly and Blachut (1991) is good with both |
| NASA (1969); Wagner et al. (2018b); Evkin (2019) | They are generally more conservative; |
| | Not sensitive to imperfection; |
| | Less precise predictions for spherical caps than complete spheres; |
| | Thin-walled shells ($\lambda > 10$) are recommended using these models |

relatively feasible results when R/t is lower than 50 and a more conservative prediction when R/t is larger than 75 for both models. It is also worth to be noticed that the results from the two formulations present very similar patterns on $\lambda$ (circled in red line): both of them show a relatively higher prediction for the data in the range $\lambda > 35$. The similar distribution on $R/t$ and $\lambda$ indicates the models may share some similarities in a certain way. The first reason for the patterns is models resemble the forms. Taking a closer look at Equations (11) and Equations (12–14), we can find the two formulas are both controlled by the value of $P_e/P_y$, and the different constants lead to various results but share some resemblance. Moreover, the coefficients in the models are constants which means the value of imperfections will not affect the calculated buckling pressure. However, the data we circled with a red line show a relatively large imperfection value (Zhang et al. 2017; Zhang et al. 2018a) which leads to a lower experiment result even if the parameters are the same. Therefore, it explains why the prediction values are larger than the real buckling pressure in these data.

Similar results obtained in Figures 8 and 9 are from the RS code and formula by Galletly and Blachut (1991), respectively. As can be seen from the figure, the results have shown they are highly imperfection-sensitive equations. The experiment data in red and green are with relatively higher imperfection values as we mentioned before, and the prediction of these data shows a large deviation from actual buckling pressure.

Figures 10–12 present the results given by Equations (17), (19) and (20) respectively. As shown in the figures, these three formulas share a very similar pattern. First, they have shown conservative predictions because they are based on the lower bound experiment results, and Equation (17) is the most conservative. Besides, they have shown relatively better predictions when $\lambda$ is in the Huang range, which means they are more suitable for thin shells. The main reason to explain the phenomenon is that linear elastic and isotropic material behaviour is required. However, the experiment results in the Budiansky range are deeply influenced by the material plasticity and, therefore, don't comply with the requirements. Besides, the boundary condition required by the equation is strictly clamped, which is another factor that caused the situation.

## 6. Conclusion

The conclusion of the comparative study on externally pressurised imperfect spherical shells may be summarised in the following paragraphs and Table 5:

1. To predict the collapse pressure of externally pressurised imperfect shells, it has been shown in the paper that the model presented by DNV (2021) obtained the best results with a mean value of 0.99 and COV of 0.19. The model from NASA (1969) presented the worst prediction with 1.64 and 0.37.

2. Models presented by DNV (2021) and ABS (2021 ) have shown similar distribution patterns due to the resemblance in the equation structure. Moreover, since the models contain empirical constant coefficients, the predictions will not be affected by the imperfection changes. Therefore, the requirement of maximum imperfection tolerance should be satisfied as an a priori condition.

3. The equations given by RS code (2018) and Galletly and Blachut (1991) are highly imperfection-sensitive models. The predictions would be much more conservative than the experiment results when the imperfection value grows. Therefore, the specimens with bad manufactural defects are not recommended for using these models

4. The models presented by NASA (1969), Wagner et al. (2018b) and Evkin (2019) have shown relatively conservative predictions than the others. They obtained less precise results predicting spherical caps than complete spheres because the requirement of strict boundary conditions is hard to be satisfied. Moreover, the calculations imply that they are more suitable for shells with large $\lambda$ (thin-walled shells) because these models are sensitive to material plasticity.

## Disclosure statement

No potential conflict of interest was reported by the author(s).

## ORCID

*Liang Zhao* http://orcid.org/0000-0002-1568-990X

**References**

American Bureau of Shipping [ABS]. 2021. Rules for building and classing underwater vehicles, system and hyperbaric facilities. Houston: ABS.

Arbelo MA, Degenhardt R, Castro SGP, Zimmermann R. 2014. Numerical characterization of imperfection sensitive composite structures. Compos Struct. 108:295–303. doi:10.1016/j.compstruct.2013.09.041.

Bagheri H, Kiani Y, Bagheri N, Eslami MR. 2022. Free vibrations of functionally graded material cylindrical shell closed with two spherical caps. Ships Offsh Struct. 17(4):939–951. doi:10.1080/17445302.2021.1889169.

Błachut J. 2015. Locally flattened or dented domes under external pressure. Thin-Walled Struct. 97:44–52. doi:10.1016/j.tws.2015.08.022.

Das PK, Thavalingam A, Bai Y. 2003. Buckling and ultimate strength criteria of stiffened shells under combined loading for reliability analysis. Thin-Walled Struct. 41(1):69–88. doi:10.1016/S0263-8231(02)00093-9.

Det Norske Veritas [DNV]. 2021. Rules for classification of underwater technology. Oslo: DNV.

Evkin A. 2019. Dynamic energy barrier estimation for spherical shells under external pressure. Int J Mech Sci. 160:51–58. doi:10.1016/j.ijmecsci.2019.06.028.

Evkin A, Krasovsky VL, Manevich LI. 1978. Stability of longitudinally compressed cylindrical shells under quasi-static local disturbances. Mech Sol. 13(6):83–88.

Evkin A, Lykhachova OV. 2017. Energy barrier as a criterion for stability estimation of spherical shell under uniform external pressure. Int J Solids Struct. 118–119:14–23. doi:10.1016/j.ijsolstr.2017.04.026.

Evkin A, Lykhachova OV. 2019. Design buckling pressure for thin spherical shells: development and validation. Int J Solids Struct. 156–157:61–72. doi:10.1016/j.ijsolstr.2018.06.035.

Galletly GD, Blachut J. 1991. Buckling design of imperfect welded hemispherical shells subjected to external pressure. Proc Inst Mech Eng C J Mech Eng Sci. 205(3):175–188. doi:10.1243/PIME_PROC_1991_205_108_02.

Galletly GD, Blachut J, Kruzelecki J. 1987. Plastic buckling of imperfect hemispherical shells subjected to external pressure. Proc Inst Mech Eng C J Mech Eng Sci. 201(3):153–170. doi:10.1243/PIME_PROC_1987_201_103_02.

Huang N-C. 1964. Unsymmetrical buckling of thin shallow spherical shells. J Appl Mech. 31(3):447–457. doi:10.1115/1.3629662.

Kołodziej S, Marcinowski J. 2018. Experimental and numerical analyses of the buckling of steel, pressurized, spherical shells. Adv Struct Eng. 21(16):2416–2432. doi:10.1177/1369433218774371.

Krenzke MA, Kiernan TJ. 1963. Test of stiffened and unstiffened machined spherical shells under external hydrostatic pressure. David Taylor Model Basin. Report 1741, S-R0110101.

NASA. 1969. Buckling of thin-walled doubly-curved shells. NASA space vehicle design criteria (structures). Washington (DC): NASA. Report No.: NASA SP-8032.

Paliy OM. 1991. Weight characteristics, reliability and operational safety of deep-sea submersible hulls. International Symposium on Marine Structures (ISM'91); Sept 13–14. Shang Hai, China. p. 197–199.

Pan BB, Cui WC. 2010. An overview of buckling and ultimate strength of spherical pressure hull under external pressure. Mar Struct. 23(3):227–240. doi:10.1016/j.marstruc.2010.07.005.

Pan BB, Cui WC. 2011. A comparison of different rules for the spherical pressure hull of deep manned submersibles. J Sh Mech. 15:276–285.

Pan BB, Cui WC, Shen YS. 2012. Experimental verification of the new ultimate strength equation of spherical pressure hulls. Mar Struct. 29(1):169–176. doi:10.1016/j.marstruc.2012.05.007.

Russian Maritime Register of Shipping [RS]. 2018. Rules for the classification and construction of manned submersibles. Saint Petersburg: RS.

Thompson JMT, Sieber J. 2016. Shock-sensitivity in shell-like structures: With simulations of spherical shell buckling. Int J Bifurcation Chaos. 26(02):1630003. doi:10.1142/S0218127416300032.

Wagner HNR, Hühne C, Khakimova R. 2018a. Towards robust knockdown factors for the design of conical shells under axial compression. Int J Mech Sci. 146–147:60–80. doi:10.1016/j.ijmecsci.2018.07.016.

Wagner HNR, Hühne C, Niemann S. 2018b. Robust knockdown factors for the design of spherical shells under external pressure: development and validation. Int J Mech Sci. 141:58–77. doi:10.1016/j.ijmecsci.2018.03.029.

Wagner HNR, Hühne C, Niemann S, Khakimova R. 2017. Robust design criterion for axially loaded cylindrical shells - simulation and validation. Thin-Walled Struct. 115:154–162. doi:10.1016/j.tws.2016.12.017.

Wang F, Zhang S, Yu S, Du Q, Zhang J, Jiang Z, Cui W. 2019. Design and analysis on a model sphere made of maraging steel to verify the applicability of the current design code. Ships Offsh Struct. 14(1):86–94. doi:10.1080/17445302.2018.1481627.

Wang Y, Tang W, Zhang J, Zhang S, Chen Y. 2019. Buckling of imperfect spherical caps with fixed boundary under uniform external pressure. Mar Struct. 65:1–11. doi:10.1016/j.marstruc.2019.01.004.

Wang Y, Zhang J, Tang W. 2020. Buckling performances of spherical caps under uniform external pressure. J Mar Sci Appl. 19(1):96–100. doi:10.1007/s11804-020-00125-7.

Zhang J, Dai M, Wang F, Tang W, Zhao X, Zhu Y. 2022. Theoretical and experimental study of the free hydroforming of egg-shaped shell. Ships Offsh Struct. 17(2):257–267. doi:10.1080/17445302.2020.1827637.

Zhang J, Gao J, Wang WB, Tang WX, Zhou T. 2015. Investigation on mechanical properties of deep-sea spherical pressure hull. Shipbuild China. 56(4):129–140.

Zhang J, Wang X, Tang W, Wang F, Zhu Y. 2021. Non-linear collapse behavior of externally pressurized resin toroidal and cylindrical shells: numerical and experimental studies. Ships Offsh Struct. 16(5):529–545. doi:10.1080/17445302.2020.1745546.

Zhang J, Wang Y, Wang F, Tang W. 2018b. Buckling of stainless-steel spherical caps subjected to uniform external pressure. Ships Offsh Struct. 13(7):779–785. doi:10.1080/17445302.2018.1459358.

Zhang J, Zhang M, Tang W, Wang WB, Wang M. 2017. Buckling of spherical shells subjected to external pressure: A comparison of experimental and theoretical data. Thin-Walled Struct. 111:58–64. doi:10.1016/j.tws.2016.11.012.

Zhang J, Zhang Y, Wang F, Zhu Y, Cui W, Chen Y, Jiang Z. 2019. Experimental and numerical studies on the buckling of the hemispherical shells made of maraging steel subjected to extremely high external pressure. Int J Press Vessels Pip. 172:56–64. doi:10.1016/j.ijpvp.2019.03.016.

Zhang M, Zhang J, Tang WX, Wang WB, Gao J. 2018a. Experimental and theoretical investigation on buckling of spherical shells. J Jiangsu Univer Sci Technol (Natural Science Edition). 32(5):627–632.

Zhao L, Bai Y, Wang F, Bai J. 2022. Path planning for autonomous surface vessels based on improved artificial fish swarm algorithm: a further study. Ships Offsh Struct. 1–13. doi:10.1080/17445302.2022.2116765.

Zhao L, Wang F, Bai Y. 2022. Route planning for autonomous vessels based on improved artificial fish swarm algorithm. Ships Offsh Struct. 1–10. doi:10.1080/17445302.2022.2081423.

Zhao Z, Zhang P, Zhou S, Fan X. 2022. Collapse pressure of randomly corroded spherical shell. Ocean Eng. 246:110604. doi:10.1016/j.oceaneng.2022.110604.

Zhu Y, Guan W, Wang H, Zhao M, Zhang J. 2021. Buckling of spherical shells with pitting corrosion under external pressure. Ships Offsh Struct. 1–10. doi:10.1080/17445302.2021.2000266.

Zhu Y, Zhang J, Yu J, Zhou X, Zhao X, Yin B, Tang W. 2020. Buckling of externally pressurized corroded spherical shells with wall-thickness reduction in local region. Int J Press Vessels Pip. 188:104231. doi:10.1016/j.ijpvp.2020.104231.

Zhu Y, Zhang Y, Zhao X, Zhang J, Xu X. 2019. Elastic–plastic buckling of externally pressurised hemispherical heads. Ships Offsh Struct. 14(8):829–838. doi:10.1080/17445302.2018.1564541.

Zoelly R. 1915. Ueber ein Knickungsproblem an der Kugelschale [about a buckling problem on the spherical shell] [dissertation]. Zürich: Eidgenössische Technische Hochschule Zürich.

## Appendix. Experiment Data for Spherical Shells

### A1.#Krenzke and Kiernan (1963)

The results by Krenzke and Kiernan listed here are from model S-1 to SS-26 according to the report.

| $\sigma_y$ (Mpa) | $E$ (Gpa) | $R/t$ | $\lambda$ | $\phi$ (rad) | $P_{exp}$ (Mpa) |
|---|---|---|---|---|---|
| 551.58 | 74.46 | 10.36 | 11.70 | 3.14 | 98.60 |
| 551.58 | 74.46 | 16.53 | 14.78 | 3.14 | 58.61 |
| 551.58 | 74.46 | 40.16 | 23.04 | 3.14 | 20.68 |
| 551.58 | 74.46 | 76.92 | 31.89 | 3.14 | 10.34 |
| 551.58 | 74.46 | 10.64 | 5.92 | 1.05 | 97.73 |
| 551.58 | 74.46 | 10.64 | 5.94 | 1.05 | 98.25 |
| 551.58 | 74.46 | 16.39 | 7.39 | 1.05 | 58.61 |
| 551.58 | 74.46 | 16.95 | 7.47 | 1.05 | 56.36 |
| 551.58 | 74.46 | 41.67 | 11.62 | 1.05 | 19.99 |
| 551.58 | 74.46 | 41.67 | 6.05 | 0.52 | 20.34 |
| 551.58 | 74.46 | 83.33 | 8.43 | 0.52 | 7.58 |
| 551.58 | 74.46 | 83.33 | 8.46 | 0.52 | 7.52 |
| 551.58 | 74.46 | 10.53 | 3.06 | 0.52 | 99.11 |
| 551.58 | 74.46 | 10.64 | 3.07 | 0.52 | 98.08 |
| 551.58 | 74.46 | 16.67 | 3.85 | 0.52 | 56.54 |
| 551.58 | 74.46 | 16.67 | 3.85 | 0.52 | 55.85 |
| 551.58 | 74.46 | 40.00 | 5.95 | 0.52 | 20.17 |
| 551.58 | 74.46 | 40.00 | 5.98 | 0.52 | 19.82 |
| 551.58 | 74.46 | 83.33 | 8.43 | 0.52 | 7.38 |
| 551.58 | 74.46 | 83.33 | 8.43 | 0.52 | 7.45 |
| 551.58 | 74.46 | 10.53 | 2.30 | 0.39 | 126.86 |
| 551.58 | 74.46 | 10.64 | 2.31 | 0.39 | 125.48 |
| 551.58 | 74.46 | 16.39 | 2.88 | 0.39 | 59.98 |
| 551.58 | 74.46 | 16.67 | 2.89 | 0.39 | 57.36 |
| 551.58 | 74.46 | 40.00 | 4.46 | 0.39 | 17.10 |
| 551.58 | 74.46 | 40.00 | 4.47 | 0.39 | 17.55 |
| 551.58 | 74.46 | 76.92 | 6.28 | 0.39 | 7.31 |
| 551.58 | 74.46 | 76.92 | 6.31 | 0.39 | 7.27 |
| 551.58 | 74.46 | 142.86 | 8.48 | 0.39 | 2.45 |
| 551.58 | 74.46 | 166.67 | 8.95 | 0.39 | 2.00 |

### A2.#Pan et al. (2012)

| $\sigma_y$ (Mpa) | $E$ (Gpa) | $R/t$ | $\lambda$ | $\phi$ (rad) | $P_{exp}$ (Mpa) |
|---|---|---|---|---|---|
| 925.00 | 110.00 | 29.67 | 19.80 | 3.14 | 56.00 |
| 925.00 | 110.00 | 26.08 | 18.57 | 3.14 | 58.29 |
| 890.00 | 110.00 | 25.88 | 18.50 | 3.14 | 57.80 |
| 888.33 | 110.00 | 26.85 | 18.84 | 3.14 | 55.00 |

### A3.#Zhang et al. (2017)

| $\sigma_y$ (Mpa) | $E$ (Gpa) | $R/t$ | $\lambda$ | $\phi$ (rad) | $P_{exp}$ (Mpa) |
|---|---|---|---|---|---|
| 246.10 | 190.70 | 175.94 | 48.40 | 3.14 | 1.71 |
| 246.10 | 190.70 | 171.67 | 47.81 | 3.14 | 1.96 |
| 246.10 | 190.70 | 174.08 | 48.14 | 3.14 | 1.77 |
| 246.10 | 190.70 | 185.91 | 49.75 | 3.14 | 1.33 |
| 246.10 | 190.70 | 179.19 | 48.84 | 3.14 | 1.59 |
| 291.60 | 188.20 | 105.52 | 37.40 | 3.14 | 3.18 |
| 291.60 | 188.20 | 103.77 | 37.09 | 3.14 | 4.50 |
| 291.60 | 188.20 | 103.37 | 37.02 | 3.14 | 4.69 |
| 291.60 | 188.20 | 104.72 | 37.26 | 3.14 | 3.97 |

### A4.#Zhang et al. (2018a)

| $\sigma_y$ (Mpa) | $E$ (Gpa) | $R/t$ | $\lambda$ | $\phi$ (rad) | $P_{exp}$ (Mpa) |
|---|---|---|---|---|---|
| 310.00 | 193.00 | 146.32 | 43.98 | 3.14 | 2.14 |
| 310.00 | 193.00 | 138.43 | 42.78 | 3.14 | 2.93 |
| 310.00 | 193.00 | 139.62 | 42.96 | 3.14 | 2.32 |
| 310.00 | 193.00 | 150.43 | 44.59 | 3.14 | 2.17 |

### A5.#Wang, Zhang, et al. (2019)

| $\sigma_y$ (Mpa) | E (Gpa) | R/t | $\lambda$ | $\phi$ (rad) | $P_{exp}$ (Mpa) |
| --- | --- | --- | --- | --- | --- |
| 1699 | 180.00 | 28.91 | 19.5 | 3.14 | 118.00 |

### A6.#Zhu et al. (2019)

| $\sigma_y$ (Mpa) | E (Gpa) | R/t | $\lambda$ | $\phi$ (rad) | $P_{exp}$ (Mpa) |
| --- | --- | --- | --- | --- | --- |
| 205.00 | 193.00 | 136.20 | 30.10 | 1.57 | 2.71 |
| 205.00 | 193.00 | 139.27 | 30.44 | 1.57 | 2.48 |
| 205.00 | 193.00 | 139.46 | 30.46 | 1.57 | 2.59 |
| 205.00 | 193.00 | 144.75 | 31.03 | 1.57 | 2.49 |
| 205.00 | 193.00 | 141.57 | 30.69 | 1.57 | 2.36 |

### A7.#Zhang et al. (2018b)

| $\sigma_y$ (Mpa) | E (Gpa) | R/t | $\lambda$ | $\phi$ (rad) | $P_{exp}$ (Mpa) |
| --- | --- | --- | --- | --- | --- |
| 335.408 | 159.00 | 88.05 | 15.44 | 0.94 | 5.28 |
| 335.408 | 159.00 | 86.95 | 15.35 | 0.94 | 5.55 |
| 335.408 | 159.00 | 86.78 | 15.33 | 0.94 | 5.26 |
| 335.408 | 159.00 | 87.28 | 15.38 | 0.94 | 5.58 |
| 335.408 | 159.00 | 86.53 | 15.31 | 0.94 | 5.36 |
| 335.408 | 159.00 | 87.03 | 15.35 | 0.94 | 5.65 |

### A8.#Zhang et al. (2019)

| $\sigma_y$ (Mpa) | E (Gpa) | R/t | $\lambda$ | $\phi$ (rad) | $P_{exp}$ (Mpa) |
| --- | --- | --- | --- | --- | --- |
| 2100 | 182.00 | 26.32 | 13.27 | 1.57 | 139.00 |

### A9.#Kolodziej and Marcinowski (2018)

| $\sigma_y$ (Mpa) | E (Gpa) | R/t | $\lambda$ | $\phi$ (rad) | $P_{exp}$ (Mpa) |
| --- | --- | --- | --- | --- | --- |
| 261.71 | 210.00 | 997.79 | 81.21 | 1.57 | 0.098 |
| 261.71 | 210.00 | 1010.62 | 81.73 | 1.57 | 0.100 |
| 261.71 | 210.00 | 1000.96 | 81.34 | 1.57 | 0.100 |
| 261.71 | 210.00 | 1005.44 | 81.52 | 1.57 | 0.099 |
| 261.71 | 210.00 | 996.52 | 81.15 | 1.57 | 0.100 |
| 314.1 | 210.00 | 630.52 | 64.55 | 1.57 | 0.393 |
| 314.1 | 210.00 | 631.72 | 64.61 | 1.57 | 0.393 |
| 314.1 | 210.00 | 625.00 | 64.27 | 1.57 | 0.356 |
| 314.1 | 210.00 | 630.52 | 64.55 | 1.57 | 0.354 |
| 314.1 | 210.00 | 633.33 | 64.70 | 1.57 | 0.355 |
| 284.63 | 210.00 | 460.31 | 55.16 | 1.57 | 0.484 |
| 284.63 | 210.00 | 458.54 | 55.05 | 1.57 | 0.496 |
| 284.63 | 210.00 | 471.78 | 55.84 | 1.57 | 0.427 |
| 284.63 | 210.00 | 472.33 | 55.87 | 1.57 | 0.439 |
| 284.63 | 210.00 | 469.83 | 55.72 | 1.57 | 0.423 |
| 294.29 | 210.00 | 325.91 | 46.41 | 1.57 | 0.963 |
| 294.29 | 210.00 | 327.65 | 46.53 | 1.57 | 1.032 |
| 294.29 | 210.00 | 324.75 | 46.33 | 1.57 | 1.076 |
| 294.29 | 210.00 | 324.75 | 46.33 | 1.57 | 1.062 |
| 294.29 | 210.00 | 324.75 | 46.33 | 1.57 | 1.081 |